PHYSICAL REVIEW B **82**, 100410(R) (2010)

Evolution of spin-wave modes in magnetic tunnel junction nanopillars

Zhongming Zeng,* Kwun Hung Cheung, and H. W. Jiang
Department of Physics and Astronomy, University of California at Los Angeles, Los Angeles, California 90095, USA

I. N. Krivorotov
Department of Physics and Astronomy, University of California, Irvine, California 92697, USA

J. A. Katine
Hitachi Global Storage Technologies, San Jose, California 95135, USA

V. Tiberkevich and A. Slavin
Department of Physics, Oakland University, Rochester, Michigan 48309, USA
(Received 9 July 2010; published 17 September 2010)

We use spin-torque-driven ferromagnetic resonance to study the mode structure of spin waves in elliptically-shaped MgO-based magnetic tunnel junction (MTJ) nanopillars with different aspect ratios (AR) of a semiminor axes of <50 nm and semimajor axes of <100 nm. We find that only one quasiuniform precession mode exists in the small AR samples, whereas, in the samples with large ARs, precession evolves into multiple modes, i.e., a quasiuniform mode and an additional nonuniform mode are simultaneously observed. The spatially nonuniform mode is a spin-wave mode localized in the edge regions, which can be well understood by considering the pinning conditions at the lateral boundaries. The appearance of the nonuniform modes results in the increase in the critical switching current density (J_c) in MTJ nanopillars.

DOI: 10.1103/PhysRevB.82.100410 PACS number(s): 75.78.−n, 75.30.Ds, 76.50.+g

MgO-based magnetic tunnel junctions (MTJs) have been extensively investigated both because of their interesting fundamental physical properties and because of their potential for applications in magnetic sensors, spin-torque- (ST-) based memories, and microwave oscillators.[1–8] In order to realize such devices, it is crucial to understand magnetization dynamics in confined magnetic materials. Brillouin light scattering,[9] magneto-optical techniques,[10] ferromagnetic resonance (FMR),[11] and ST-FMR (Ref. 12) have been applied to study the magnetization dynamics in various magnetic nanostructures. Among them, ST-FMR enables the direct study of the magnetization dynamic properties of an individual nanoscale ferromagnet, such as magnetic damping and spin-transfer torques.[6,7,12–16] However, most of the previous analyses assumed uniform equilibrium and were not systematically correlated with the size and shape of the samples. It is well known that the sample size and shape play a significant role in magnetization reversal of confined magnetic structures but how they affect the magnetization dynamics such as precession mode is still poorly understood. The effect of size on magnetization dynamics has been studied in arrays of dots[17,18] and stripes.[19] In these studies uniform modes and nonuniform modes were observed in large area samples. Very recently, Helmer *et al.*[20] reported the quantized spin-wave modes in rectangular-shaped MTJ nanopillars with different sizes. However, so far there has been no systematic investigation of the shape variation in the precession modes in nanoscale MTJs.

In this Rapid Communication we investigate the evolution of the precession modes in MgO-based MTJ nanopillars by using the ST-FMR technique. In this implementation, elliptical-shaped nanopillars of various aspect ratios (ARs), with semiminor axes of <50 nm and semimajor axes of <100 nm, are chosen because elliptical elements have been considered an interesting system for examining static and dynamic magnetic properties. One of the reasons why we focus on nanopillars with such small dimensions is to minimize the size effect on mode structures. We find that shape variation in nanopillars has significant influences in the precession of magnetization, which can be of great help in the design and performance of MTJ devices.

Our nanopillars are fabricated from stacks of composition PtMn(15)/CoFe(2.5)/Ru(0.85)/CoFeB(2.4)/MgO(0.96)/CoFeB(1.8) (thickness in nm). The completed stack is annealed for 2 h at 300 °C at 1 T. These layered stacks are fabricated into elliptical nanopillars of eight sizes with various ARs: 95×65 nm^2, 115×65 nm^2, 135×65 nm^2, 160×65 nm^2, 190×65 nm^2, 110×50 nm^2, 140×85 nm^2, 170×90 nm^2 nominally, hereafter called S1 to S8, respectively, and the aspect ratio is defined as AR$=L/S$ (L and S are the length in the long and short axes of the elliptical sample, respectively). Note that S1–S5 are designed to investigate the shape variation effect on precession modes and S6–S8 are designed to study the size effect on mode structures. All samples have a tunnel magnetoresistance (TMR) of around 150% and a resistance-area product of ~10 Ω μm^2 in the parallel state. The TMR ratio, resistance at antiparallel (R_{AP}) and parallel (R_P) states, the coercivity (H_c) of the free layer, and the offset field (H_{off}, the coupling field between the free layer and the pinned layer) for various devices are summarized in Table I. It can be seen that the H_c values of the samples are consistent with the in-plane anisotropy, as expected from the shape variation. These data indicate that the samples have high-enough quality to support the further analysis of the evolution of the mode structures. For ST-FMR measurements, a microwave-frequency current (I_{rf}) is applied to a MTJ through a bias T and the magnetic field (H) is applied in the in-plane hard-axis direction (the misalignment of the field should not exceed 2°). The ST-FMR signal (V_{mix}) is recorded by sweeping the magnetic field and fre-

TABLE I. TMR ratio, resistance at antiparallel (R_{AP}) and parallel (R_P), coercivity (H_c) of the free layer, and offset field (H_{off}) for various devices with different ARs. TMR ratio is defined as TMR $=100\times(R_{AP}-R_P)/R_P$.

	Nominal size (nm^2)	AR	R_{AP} (kΩ)	R_P (kΩ)	TMR (%)	H_c (Oe)	H_{off} (Oe)
S1	95×65	1.5	6.51	2.65	146	5	34
S2	115×65	1.8	4.82	1.91	152	15	46
S3	135×65	2.1	3.99	1.56	155	52	46
S4	160×65	2.5	3.04	1.22	149	67	50
S5	190×65	2.9	2.43	0.98	148	98	47
S6	110×50	2.2	6.76	2.73	148	8	49
S7	140×85	1.7	2.49	0.99	152	16	47
S8	170×90	1.9	1.92	0.74	157	66	52

quency in the range of 4–10 GHz.[12] Note that the rf current is chosen to be as low as possible in order to minimize the change in the ST-FMR line shape, yet high enough to obtain sufficient signal-to-noise ratio. The magnetization precession frequency is the quantity of interest in this study and the amplitude can therefore be neglected.

Figures 1(a)–1(f) show contour plots of the frequency spectra for representative samples (S1–S5) with various ARs after subtraction of a background voltage. The two-dimensional contour plots are generated from individual spectra acquired at various frequencies. Note that the amplitudes are normalized for comparison. The samples with small ARs (S1–S3) exhibit a single precession mode (quasiuniform precession mode, M0), whereas for the samples with large ARs (S4 and S5), a quasiuniform mode and an additional mode (nonuniform mode, M1) are observed, as shown in Fig. 2(a). This effect is not due to random sample variation because nominally identical devices show similar spectra as shown in Figs. 1(b) and 1(f). It is also observed that, in S1, no low-field component in M0 is found due to the extremely small coercivity of the free layer. In other samples mode M0 has a V shape with minima at both positive and negative fields (the exact minima is not shown in our data due to the frequency limit) and the minima are interpreted as corresponding to the saturation of the free-layer magnetization along the hard axis (only frequency in the high-field region is considered in this study). On the other hand, the appearance of mode M1 is very sensitive to the sample shape because it is a localized spin-wave mode arising from spatial confinement effects. The evolution of this spin-wave mode will be discussed later on. This mode may originate from the inhomogeneity of the internal magnetic field caused by the demagnetizing effects brought about by the sample shape. The absence of M1 in S2 and S3 is expected since the demagnetizing field and the resulting equilibrium in small AR is homogeneous. The appearance of M1 in S4 and S5 indicates different demagnetizing fields exist in the free layer with different resonance conditions.

All modes shift to higher frequencies at $|H|>400$ Oe and the nonuniform mode (M1) disappear when further increasing the field because edge-domain contributions are significant mainly in the low-field region. It is interestingly found

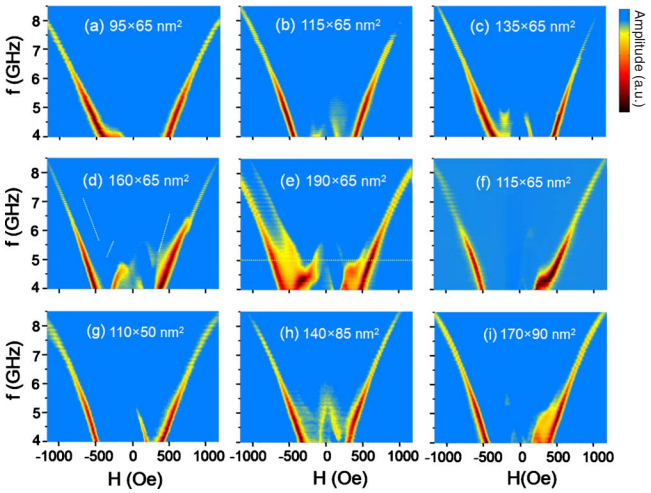

FIG. 1. (Color online) Contour plots of spectra for samples with various aspect ratios: (a) S1:95×65, [(b) and (f)] S2: 115×65, (c) S3: 135×65, (d) S4: 160×65, (e) S5: 190×65, (g) S6: 110×50, (h) S7: 140×85, and (i) S8: 170×90 (nm^2). The scale bar represents the normalized amplitude. The nonuniform modes are presented in (d) and (e) but the amplitude of M1 in (d) is relatively weak compared to that of M0, and the dashed line in (d) is guide to the eye for M1. The pairs S6 and S1, S7 and S4, and S8 and S5, have similar area with different AR.

that at high field the frequency of M0 shifts to lower frequencies with increasing nanopillar ARs at a given field, as shown Fig. 2(b). For instance, at $H=+780$ Oe, the precession frequency decreases from 6.82 GHz for S2 to 6.28 GHz for S5. This correlation could be related to the inhomogenous demagnetization.

One may argue that the presence of mode M1 presented above may come from size effect since it plays an important role in determining the magnetic properties in nanoscale magnetic structures. Three samples (S6–S8) are designed to clarify how size variations under 200 nm affect the mode structures, e.g., S6 has a similar area but different AR as S1, and similarly for S7 vs S4, and S8 vs S5. Figures 1(g)–1(i) show the contour plots of the frequency spectra for these samples. It can be easily seen that the smaller AR samples show a more quasiuniform precession behavior compared to their larger AR counterparts with similar areas. For example,

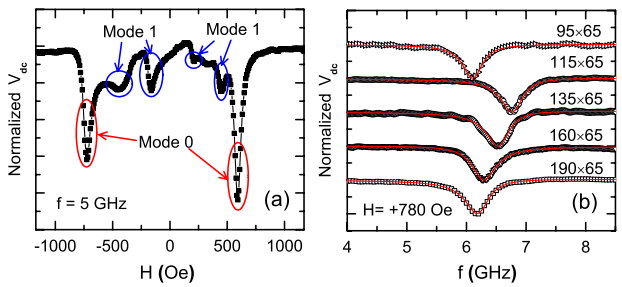

FIG. 2. (Color online) (a) A typical magnetic field-dependent ST-FMR spectra showing quasiuniform process mode (M0) and nonuniform mode (M1) of the sample S5. (b) Quasiuniform mode (M0) frequency for the samples with different AR at $H=+780$ Oe. Symbols are data and lines are fit to a combined symmetric and antisymmetric Lorenztians (Ref. 13).

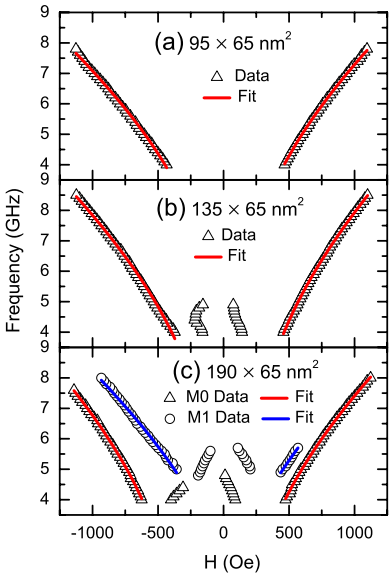

FIG. 3. (Color online) Mode frequency versus field applied to the hard axis of the samples for: (a) S1: 95×65 nm^2, (b) S3: 135×65 nm^2, and (c) S5:190×65 nm^2. Symbols are data and lines are fits for Eq. (1) and only the high-field region is considered in our study.

S7 exhibits only a quasiuniform mode, whereas S4 presents two modes. Note that when the device size is relatively large, the size effect may appear as shown in Fig. 1(i). These comparisons show clearly that shape variations have significant effect on mode structures at a given area when the sizes are less than 100×200 nm^2. Therefore, in our elliptical devices shape variations play a more important role than that of size variations in the evolution of the mode structures. Different mode structures indicate different inhomogeneities, which are related to the different pinning conditions at the lateral boundaries.

In order to better understand how the shape variations affect mode structures, the dipole-exchange dispersion of the spin-wave modes in the finite element is used in our study[21–23]

$$f=\gamma/(2\pi)\left\{\left[H-H_{anis}+\frac{2A}{M}k^2+4\pi M\left(1-\frac{1-\exp(-kd)}{kd}\right)\frac{k_x^2}{k^2}\right]\times\left[H+\frac{2A}{M}k^2+4\pi M\left(1-\frac{1-\exp(-kd)}{kd}\right)\right]\right\}^{1/2}, \quad (1)$$

where $\gamma/2\pi=2.8$ MHz/Oe is the gyromagnetic ratio, H is the magnetic field along the hard axis, H_{anis} is the in-plane anisotropy, d is the free-layer thickness, A is the exchange stiffness parameter [$A=2.84\times10^{-6}$ erg/cm^2 for 40 nm CoFeB in Ref. 24, we compare their values of $4\pi M$ (1.8 T) with ours (0.9 T), the apparent reduction in the free-layer magnetization in our case is sometimes attributed to the effect of patterning[25] and sometimes to the influence of the dipole-dipole interaction between the nanopillar magnetic layers, $A=1.6\times10^{-6}$ erg/cm^2 is found to be good for our study], and $k^2=k_x^2+k_y^2$, as discussed in Ref. 23, we choose discrete wave vectors k such that $k_x=(n_x+\Delta n_x)\pi/L$ and $k_y=(n_y+\Delta n_y)\pi/S$. Here the mode numbers (n_x and n_y) are integers starting at 0 and Δn_x (Δn_y) is a pinning parameter determined by the boundary conditions for dynamic magnetization at the pillar edges (for instances, $\Delta n_x=0$ corresponds to totally unpinned, whereas $\Delta n_x=1$ describes complete pinned). For simplicity, we will consider the x component (along the long axis of the elliptical sample) at the high-field region ($|H|>400$ Oe) in our study, i.e., $\Delta n_y=0$. Figure 3 shows some examples of Eq. (1) fits to frequency by using Δn_x and H_{anis} as fitting parameters. It can be seen that this fitting procedure gives high-quality results. These fits allow us to extract the H_{anis} values of the free layers. For S1 with small AR (1.46), $H_{anis}\approx210$ Oe, while for S3 with middle AR (2.08), $H_{anis}\approx305$ Oe, and for S5 with larger AR (2.92), $H_{anis}\approx450$ Oe. All these data are in agreement with the H_c values of the free layer obtained from the resistance-field loops as shown in Table I. Through these fits we can estimate the pinning conditions. We find that the effective pinning is considerably related to the AR and device size as shown in Fig. 4(a). When the AR are small ($\leq\sim2.2$) and the device size is also small, and the effective pining at the boundary is relatively weak, consistent with the results in Ref. 20. In this case, the demagnetizing field in these pillars is almost quasiuniform and thus only one quasiuniform mode can be detected as shown in Figs. 1(a)–1(c), 1(g), and 1(h). When the AR is large (>2.2), the effective pinning and the inhomogeneous demagnetizing field are strong, which accounts for the evolution of a spin-wave mode of dynamic magnetization precession.[26] It can also be seen that at a given size the samples with large ARs (S4 and S5) have stronger pinning than that of the samples with small ARs (S7 and S8), which indicates that shape variation plays a significant role in the evolution of spin-wave modes in our case.

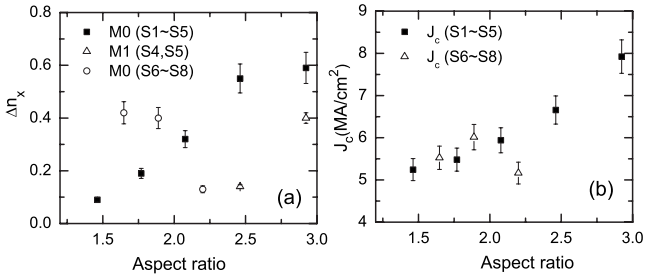

FIG. 4. (a) The effective pinning parameters (Δn_x) and (b) the critical switching current density (J_c) for various samples.

The presence of spin-wave modes implies the existence of nonuniform magnetization, which is expected to significantly affect the magnetization dynamics. One result of this effect is linewidth (Δf) broadening. Indeed, a slight increase in Δf is observed in S4 and S5 compared to that of S1–S3. But we find that the effective damping (α_{eff}) is largely unaffected by size and ARs, and we find it to be $\alpha_{eff}\approx0.015$, which is a little larger than that in Refs. 13, 14, and 24. This can be understood by considering that the thickness in our case is thinner than in their cases, consistent with other previously reported values over this thickness range.[27]

In addition, our data strongly suggest that the nonuniform

magnetization precession may influence the critical current density (J_c) in current-induced switching. The pulse current-induced switching measurements similar to the previously reported[28] are implemented to verify this issue. We measure the switching probability (P_s) at different pulse current with a 10 ns width. During the measurements a magnetic field equal to H_{off} of each sample is applied along the easy axis of the sample surface. We extract the critical switching current $I_c^{AP\to P}$ ($I_c^{P\to AP}$) corresponding to $P_s=50\%$ in switching free-layer magnetization from antiparallel (parallel) to parallel (antiparallel) states. The average critical current density is defined as $J_c=(|I_c^{AP\to P}|+|I_c^{P\to AP}|)/A$, where A is the device area. Figure 4(b) represents the J_c values for corresponding samples, showing that J_c increases significantly with AR and size, which is consistent with the effective pinning as shown in Fig. 4(a). We believe that this increase in J_c is related to the presence of the nonuniform modes. The presence of spatially nonuniform, high-order spin-wave modes would necessarily require additional energy to switch the net magnetization. The distribution of different spin-wave modes would introduce interference, alter the local conductivity and dynamically redistribute the current inside the sample. Furthermore, the coherent switching dynamics, expected for a uniform magnetization, can no longer be sustained when there is a spatial inhomogeneity. Practically, high J_c values mean that a high energy per write is needed, while, of course, reducing the energy per write is desirable in spin-torque based memory applications. Another critical challenge for ST memory is the enhancement of thermal stability. For in-plane free-layer magnetization, thermal stability is dependent on shape anisotropy, which increases with increasing AR. Optimizing these two critical parameters (minimizing write energy while maintaining thermal stability), our results show that, at a given area, samples with AR$\approx$2.0 are promising for ST-based memory.

In summary we have investigated the evolution of spin-wave modes in elliptically-shaped MgO-based MTJ nanopillars. The magnetization precession structure is sensitive to the effective pinning at the boundary, which increases with increasing aspect ratio for a given area. The appearance of the nonuniform mode results in the increase in the J_c values. These findings are important for the design and optimization of MTJ devices, such as ST-based memory and magnetic microwave oscillators.

We would like to thank Yiming Huai for fruitful discussions. This work was supported by the DARPA STT-RAM program, the Western Institute of Nanoelectronics, NSF Grants DMR-0748810 and ECCS-1002358. We also acknowledge Singulus for deposition of the magnetic multilayers.

*zhongming.zeng@gmail.com

[1] W. H. Butler, X.-G. Zhang, T. C. Schulthess, and J. M. MacLaren, Phys. Rev. B **63**, 054416 (2001).
[2] J. Mathon and A. Umerski, Phys. Rev. B **63**, 220403(R) (2001).
[3] S. S. P. Parkin, C. Kaiser, A. Panchula, P. M. Rice, B. Hughes, M. Samant, and S.-H. Yang, Nature Mater. **3**, 862 (2004).
[4] S. Yuasa, T. Nagahama, A. Fukushima, Y. Suzuki, and K. Ando, Nature Mater. **3**, 868 (2004).
[5] A. A. Tulapurkar, Y. Suzuki, A. Fukushima, H. Kubota, H. Maehara, K. Tsunekawa, D. D. Djayaprawira, N. Watanabe, and S. Yuasa, Nature (London) **438**, 339 (2005).
[6] H. Kubota, A. Fukushima, K. Yakushiji, T. Nagahama, S. Yuasa, K. Ando, H. Maehara, Y. Nagamine, K. Tsunekawa, D. D. Djayaprawira, N. Watanabe, and Y. Suzuki, Nat. Phys. **4**, 37 (2008).
[7] J. C. Sankey, Y.-T. Cui, J. Z. Sun, J. C. Slonczewski, R. A. Buhrman, and D. C. Ralph, Nat. Phys. **4**, 67 (2008).
[8] A. M. Deac, A. Fukushima, H. Kubota, J. Maehara, Y. Suzuki, S. Yuasa, Y. Nagamine, K. Tsunekawa, D. D. Djayaprawira, and N. Watanabe, Nat. Phys. **4**, 803 (2008).
[9] S. O. Demokritov and B. Hillebrands, Top. Appl. Phys. **83**, 65 (2002).
[10] A. Barman, S. Wang, J. Maas, A. R. Hawkins, S. Kwon, J. Bokor, A. Liddle, and H. Schmidt, Appl. Phys. Lett. **90**, 202504 (2007).
[11] S. Tamaru, J. A. Bain, R. J. M. van de Veerdonk, T. M. Crawford, M. Covington, and M. H. Kryder, J. Appl. Phys. **91**, 8034 (2002).
[12] J. C. Sankey, P. M. Braganca, A. G. F. Garcia, I. N. Krivorotov, R. A. Buhrman, and D. C. Ralph, Phys. Rev. Lett. **96**, 227601 (2006).
[13] G. D. Fuchs, J. C. Sankey, V. S. Pribiag, L. Qian, P. M. Braganca, A. G. G. Garcia, E. M. Ryan, Z.-P. Li, O. Ozatay, D. C. Ralph, and R. A. Buhrman, Appl. Phys. Lett. **91**, 062507 (2007).
[14] C. Wang, Y.-T. Cui, J. Z. Sun, J. A. Katine, R. A. Buhrman, and D. C. Ralph, Phys. Rev. B **79**, 224416 (2009).
[15] Y. Guan, J. Z. Sun, X. Jiang, R. Moriya, L. Gao, and S. S. P. Parkin, Appl. Phys. Lett. **95**, 082506 (2009).
[16] S. Petit, C. Baraduc, C. Thirion, U. Ebels, Y. Liu, M. Li, P. Wang, and B. Dieny, Phys. Rev. Lett. **98**, 077203 (2007).
[17] G. Gubbiotti, M. Madami, S. Tacchi, G. Carlotti, and T. Okuno, Phys. Rev. B **73**, 144430 (2006).
[18] J. M. Shaw, T. J. Silva, M. L. Schneider, and R. D. McMichael, Phys. Rev. B **79**, 184404 (2009).
[19] C. T. Boone, J. A. Katine, J. R. Childress, V. Tiberkevich, A. Slavin, J. Zhu, X. Cheng, and I. N. Krivorotov, Phys. Rev. Lett. **103**, 167601 (2009).
[20] A. Helmer, S. Cornelissen, T. Devolder, J.-V. Kim, W. van Roy, L. Lagae, and C. Chappert, Phys. Rev. B **81**, 094416 (2010).
[21] K. Yu. Guslienko and A. N. Slavin, Phys. Rev. B **72**, 014463 (2005).
[22] B. A. Kalinikos and A. N. Slavin, J. Phys. C **19**, 7013 (1986).
[23] R. McMichael and M. Stiles, J. Appl. Phys. **97**, 10J901 (2005).
[24] C. Bilzer, T. Devolder, Joo-Voo Kim, G. Counil, C. Chappert, S. Cardoso, and P. P. Freitas, J. Appl. Phys. **100**, 053903 (2006).
[25] S. Cornelissen, L. Bianchini, A. Helmer, T. Dvolder, Joo-Von Kim, M. Op de Beeck, W. Van Roy, L. Lagae, and C. Chappert, J. Appl. Phys. **105**, 07B903 (2009).
[26] R. D. McMichael and B. B. Maranville, Phys. Rev. B **74**, 024424 (2006).
[27] S. M. Rezende, A. Azevedo, M. A. Lucena, and F. M. de Aguiar, Phys. Rev. B **63**, 214418 (2001).
[28] R. H. Koch, J. A. Katine, and J. Z. Sun, Phys. Rev. Lett. **92**, 088302 (2004).